Ultrafast intersystem crossing in xanthone from wavepacket dynamics simulations

Marc Alías-Rodríguez,[1] Coen de Graaf,[1,2] and Miquel Huix-Rotllant[3,a)]
[1)] *Departament de Química Física i Inorgànica, Universitat Rovira i Virgili, Marcel·lí Domingo 143007 Tarragona, Catalunya, Spain.*
[2)] *ICREA, Passeig Lluís Companys 23, Barcelona, Spain*
[3)] *Aix-Marseille Univ, CNRS, ICR, Marseille, France.*

Most aromatic ketones containing first-row elements undergo unexpectedly fast intersystem crossing in few tens of picoseconds and a quantum yield close to unity. Among them, xanthone (9H-xanthen-9-one) possesses one of the fastest intersystem crossing rates of ∼1.5 ps, despite containing only first-row elements. The exact mechanism of this unusually fast singlet-triplet transition is still under debate. Here, we perform a complete wavepacket dynamics simulation of the internal conversion and intersystem crossing reactions of xanthone in the gas phase. We show that xanthone follows El-Sayed's rule for intersystem crossing. From the second singlet excited state, the mechanism is sequential: (i) an internal conversion between singlets $^1\pi\pi^* \rightarrow {}^1n\pi^*$ (85 fs), (ii) an intersystem crossing $^1n\pi^* \rightarrow {}^3\pi\pi^*$ (2.0 ps), and (iii) an internal conversion between triplets $^3\pi\pi^* \rightarrow {}^3n\pi^*$ (602 fs). Each transfer finds its origin in a barrierless access to electronic state intersections. These intersections are close to minimum energy structures, allowing for efficient radiationless transitions from the initial singlet state to the triplets.

Aromatic ketones are well known for their phosphorescent properties due to an efficient intersystem crossing (ISC)[1–4] non-radiative transfer between singlet and triplet excited states of the type $n\pi^*$ and $\pi\pi^*$. The n orbital corresponds to the carbonyl lone pair orbital mixed with σ orbitals on the carbon bonds, while the π and π^* are a mixture of bonding and anti-bonding combinations of the atomic p_z orbitals centred on the carbonyl and the aromatic rings. According to classical photochemistry rules for ISC (known as El-Sayed's rules),[5] an efficient transition is characterized by simultaneous strong spin-orbit coupling and a small energetic gap between singlet and triplets states of dissimilar character, that is, $^1n\pi^* \rightarrow {}^3\pi\pi^*$ or $^1\pi\pi^* \rightarrow {}^3n\pi^*$. The lifetime of triplet states in aromatic ketones are reported to last from few to several tens of picoseconds, depending mainly on the energetic gap between $n\pi^*$ and $\pi\pi^*$ states. For example, acetophenone ISC rate is reported to be 42 ps,[6] benzophenone 5-10 ps,[7], anthrone 70 ps,[8] etc. This gap can be modulated or even interchanged singlet and triplet depending on the type of ketone,[8–11] solvent polarity,[12–16] temperature,[2] pressure,[17] substituents,[16,18] concentration,[19] etc.

It is currently widely accepted that vibrations play a central role in modulating the efficiency of non-radiative decays,[20] and intersystem crossings of aromatic ketones are no exception.[21–24] One of us performed one of the first wavepacket dynamics simulations in acetophenone, showing a rapid $^3n\pi^*/{}^3\pi\pi^*$ internal conversion after the $^1n\pi^* \rightarrow {}^3\pi\pi^*$ intersystem crossing.[23] Almost simultaneously, Granucci and coworkers performed a study of benzophenone using fewest-switch surface hopping, obtaining a 16 ps direct transfer from the lowest singlet to the lowest triplet, due to the mixed $n\pi^*$ and $\pi\pi^*$ character of the states.[24] Marian and coworkers have studied the ISC of thioxanthone[25–27] and xanthone[22] using Fermi Golden's rule to determine vibronic intersystem crossing rates.

The triplet quantum yield of xanthone in solution is close to unity.[12] Among the aromatic ketones, xanthone has one of the fastest intersystem crossings, estimated to be around 1-1.5 picoseconds in ethanol by femtosecond fluorescent experiments.[28–30] In these experiments, two kinetic steps of 1.5 ps and 12 ps were obtained. Two mechanisms were proposed to explain these rates: (i) sequential mechanism, with a fast $^1\pi\pi^* \rightarrow {}^3n\pi^*$ transfer in 1.5 ps and a slow component of 12 ps belonging to the internal conversion between triplets, and (ii) a branching mechanism, in which the 1.5 ps component corresponds to both the ISC $^1\pi\pi^* \rightarrow {}^3n\pi^*$ and the internal conversion $^1\pi\pi^* \rightarrow {}^1n\pi^*$, and the slow 12 ps component to the $^1n\pi^* \rightarrow {}^3\pi\pi^*$ transfer from the lowest singlet. Rai-Constapel and coworkers simulated the intersystem crossing kinetic rate in gas phase and solution of xanthone using Fermi Golden's rule.[22] In the gas phase, they obtained a fast $^1\pi\pi^* \rightarrow {}^3\pi\pi^*$ ISC of about 5 ps, and a $^1\pi\pi^* \rightarrow {}^3n\pi^*$ ISC of 200 ps, in apparent contradiction with El-Sayed's rule. As for the $^1n\pi^* \rightarrow {}^3\pi\pi^*$ ISC rate of 0.13 ps, which is 10-100 times faster than the experimental reported values. The $^1n\pi^* \rightarrow {}^3n\pi^*$ transition was estimated at ca. 330 ps. Recently, Bracker et al. extended the use of Fermi's golden rule for both the internal coversion and the intersystem crossing.[31] They results suggested that $^1\pi\pi^*$-$^3\pi\pi^*$ ISC and $^1\pi\pi^*$-^{1}nπ^* IC to be competitive transitions and proposed a unified branched mechanism.

Here, we report a quantum wavepacket dynamics of xanthone including the lowest two singlet and the four triplet excited states. The model contains all non-adiabatic and spin-orbit couplings to represent the internal conversion and intersystem crossing on the same

[a)] Electronic mail: miquel.huixrotllant@univ-amu.fr

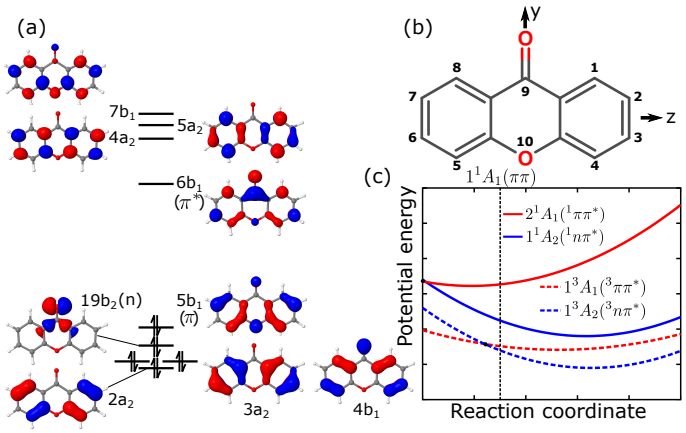

FIG. 1. Schematic structure of 9H-xanthen-9-one (xanthone) with the Cartesian axis orientation and the ring atom's numbering. On the left, the 5 highest occupied and 4 lowest unoccupied orbitals are shown tagged by the symmetry label of C_{2v}, and the short-hand notation in parenthesis. On the right, schematic diabatic potential energy surface of the two lowest singlet (solid line) and triplet (dashed line) excited states for the $n\pi^*$ (red) and $\pi\pi^*$ states (blue), where the vertical dashed line represents the Franck-Condon geometry.

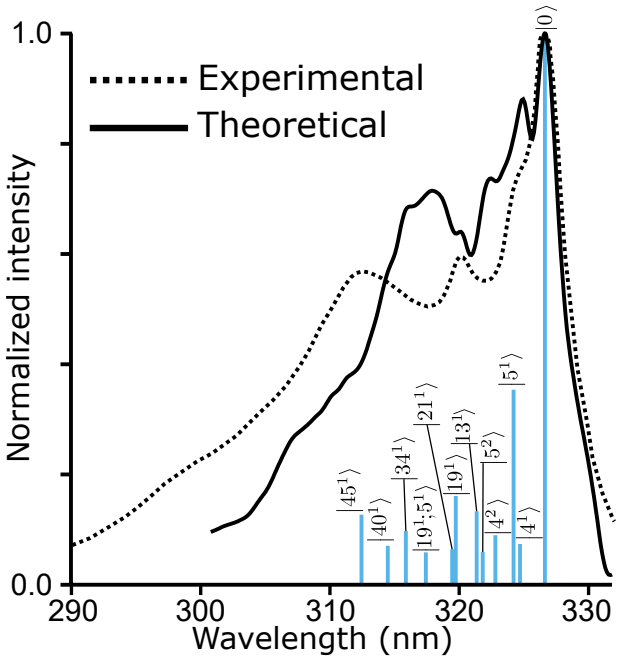

FIG. 2. Comparison of the experimental and theoretical gas phase singlet-singlet absorption spectra of xanthone for the 2^1A_1 state ($^1\pi\pi^*$) transition. Experimental data has been extracted from Ref. 33, and corresponds to the gas phase UV spectrum of xanthone recorded at 150 °C. The solid line corresponds to the Fourier transform of the numerical autocorrelation function obtained during wavepacket propagation. For analysis purposes, the stick spectrum is shown as blue vertical lines with their corresponding analys, corresponding to the Franck-Condon Herzberg-Teller vibrational expansion. All theoretical spectra have been shifted and normalized to the most intense peak of the experimental spectrum.

footing, including the effect of Duschinsky rotations.[32] The total vibronic Hamiltonian can be written as

$$\mathbf{H}(\mathbf{Q}) = [\mathbf{T}(\mathbf{Q}) + \mathbf{V}(\mathbf{Q})]\,\mathbf{1} + \mathbf{H}^{\mathrm{NA}}(\mathbf{Q}) + \mathbf{H}^{\mathrm{SO}}(\mathbf{Q})\,. \quad (1)$$

Here, $\mathbf{T}(\mathbf{Q})$ and $\mathbf{V}(\mathbf{Q})$ are the kinetic and diabatic potential energies accounting for the reorganization energy in each electronic state, and $\mathbf{H}^{\mathrm{NA}}(\mathbf{Q})$ and $\mathbf{H}^{\mathrm{SO}}(\mathbf{Q})$ are the vibronic non-adiabatic and spin-orbit couplings respectively representing the non-radiative internal conversion and intersystem crossings respectively. The explicit expressions for the Hamiltonian blocks and the parametrization are described in Sec. S1 of the supporting information.

Xanthone lowest energy state is a singlet 1^1A_1 state (using C_{2v} point group symmetry labeling, with the orientation as described in Fig. 1). At this geometry, the 1^1A_2 state is the first excited singlet, corresponding to a $19b_2 \rightarrow 6b_1$ transition (also called $^1n\pi^*$ state), which is dipole-forbidden. The second singlet excited state is the 2^1A_1 state, which is represented by a $5b_1 \rightarrow 6b_1$ transition (more commonly referred to $^1\pi\pi^*$ state), and is dipole-allowed. The vibrationally resolved absorption spectrum in gas phase for $^1\pi\pi^*$ is shown in Fig. 2 and compared to the experimental spectrum in gas phase taken from Ref. 33. The theoretical spectrum has been obtained by the Fourier transform of the autocorrelation function extracted from a wavepacket propagation on the $^1\pi\pi^*$ state with the Hamiltonian defined in Eq. 1, that is, considering the spin-orbit and vibronic couplings of $^1\pi\pi^*$ state.[34,35] For analysis purposes, we have performed a vibrational integral overlap computation using the Franck-Condon and Herzberg-Teller approximations for the diabatic $S_0 \rightarrow {}^1\pi\pi^*$ transition.[36,37] The most intense peak is the fundamental zero-zero transition $|0^0\rangle \rightarrow |0^0\rangle$, followed by two fundamental and two overtone transitions to $|4\rangle$ (mode frequency of 231.8 cm^{-1}, a_1, in-plane) and $|5\rangle$ (247.3 cm^{-1}, a_2, out-of-plane) that show up as a shoulder next to the main transition. The next vibrational transitions is represented by fundamental transitions to $|13\rangle$ (530.0 cm^{-1}, a_2, coupling mode), $|19\rangle$ (713.6 cm^{-1}, a_1, tuning mode) and $|21\rangle$ (773.3 cm^{-1}, b_1, tuning mode), while the last vibrational peak is essentially represented by fundamental transitions to $|34\rangle$ (1060.0 cm^{-1}, b_2, tuning mode), $|40\rangle$ (1248.8 cm^{-1}, a_1, tuning mode) and $|45\rangle$ (1379.0 cm^{-1}, b_2, tuning mode).

In the minimum energy structure of 1^1A_1 state (Fig. 1), the triplets 1^3A_2 and 1^3A_1 are quasi-degenerate (0.03 eV gap), 0.166 eV below the singlet 1^1A_2 state, in good agreement with the experimental value of 0.14 eV.[38] The 1^1A_2 state is only 0.06 eV below the 2^3A_1 described mainly by a $4b_1 \rightarrow 6b_1$ transition, and the triplet 1^3B_2 described mainly by a $3a_2 \rightarrow 6b_1$ is found ~0.11 eV above 1^1A_2. The 2^1A_1 state ($5b_1 \rightarrow 6b_1$) is the highest energy state, 0.4 eV above the 1^1A_2 state. Minimal energy structures of the lowest singlet and triplet states are planar of quasi-C_{2v} symmetry. As for the state crossings, on the one hand the $2^1A_1/1^1A_2$ ($^1\pi\pi^*/^1n\pi^*$) cross in

an accidental different symmetry structure of C_s resulting from the linear combination of the carbonyl symmetric stretching (essentially of a_1 symmetry) and an asymmetric stretching vibration of mostly b_1 symmetry involving the carbon atoms on the aromatic ring. On the other hand, 1^1A_2 crosses with 1^3A_1 state in a quasi-C_{2v} structure expanded through totally symmetric vibrations involving the carbonyl symmetric stretching of the aromatic rings.

Non-zero non-adiabatic coupling of A_1 and A_2 states is only occurring in distorted geometries whose point group symmetry is lowered to C_2 sub-group by means of asymmetric out-of-plane a_2 vibrations (hereafter referred as "coupling modes"). This indeed mixes $n\pi^*$ and $\pi\pi^*$ states as was shown previously for benzophenone.[24] None of the minimum energy structures or minimum energy crossing points belongs to the C_2 subgroup, and thus, only accidental different symmetry intersections are happening in xanthone. The b_1 modes are out-of-plane symmetric distortions, breaking the symmetry to the C_s sub-group in which σ_{xy} is the plane of symmetry. The lone pair orbital ($19b_2$) becomes a", while the π orbitals of b_1 symmetry become a', and thus $n\pi^*$ and $\pi\pi^*$ are uncoupled. These modes are not introducing couplings among the A_2 and A_1 states. The "tuning modes", that is, the modes that modulate the gap and describe the reorganization energy of the excited states, are of b_2 symmetry (asymmetric in-plane) and a_1 symmetry modes (symmetric in-plane). In a_1, the C_{2v} point group symmetry is maintained, whereas a symmetry breaking C_s sub-group in which σ_{yz} (that is, the molecular plane) is the plane of symmetry is observed along b_2 symmetry modes. Similar to b_1, n- and π-type orbitals fall in different symmetries and thus are uncoupled.

The spin-orbit coupling follows different symmetry rules than the non-adiabatic couplings. The singlet 2^1A_1 state mixes with triplets 1^3A_2 and 1^3B_2, but not to other 1^3A_1 or 2^3A_1 states. However, spin-vibronic coupling can activate the mixing with A_1 triplets through vibrations of a_2, b_1 and b_2 type. The 1^1A_2 on the other hand couples to triplets 1^3A_1, 2^3A_1 and 1^3B_2, and can couple to the 1^3A_2 through vibronic spin-orbit with vibrations of the type a_2, b_1 and b_2 type. Still, the vibronic spin-orbit couplings are small and thus intersystem crossing can happen only between states that are energetically close in energy. The 2^1A_1 is energetically far from the rest of the triplet manifold, while the 1^1A_2 state is energetically close to triplets of different symmetry. Thus, the latter singlet is expected to be the main state from which intersystem crossing happens for xanthone in the gas phase.

The dynamic evolution of diabatic populations is shown in Fig. 3. The simulations have been started at the 2^1A_1 state. The population of this state rapidly decays in the first 200 fs, concomitant to the 1^1A_2 population rise, indication of the fast internal conversion between the two states. This is due to the barrierless access to two $1^1A_2/2^1A_1$ accidental different symmetry intersections. In this process, 80% of the 2^1A_1 is transferred to 1^1A_2. Still, 20% of the population remains trapped in 2^1A_1, and decays at a slower rate. The 1^1A_2 being the most populated state after 200 fs rapidly decays to the triplets. Initially, the intersystem crossing is mainly due to the $1^1A_2 \rightarrow 1^3A_1$ transition and to a lesser extent $1^1A_2 \rightarrow 2^3A_1$. These are the only contributions to the build up of triplet populations, consistent thus with El-Sayed's rule for intersystem crossing. The transfer between triplets slowly builds up the population on the lowest triplet 1^3A_2.

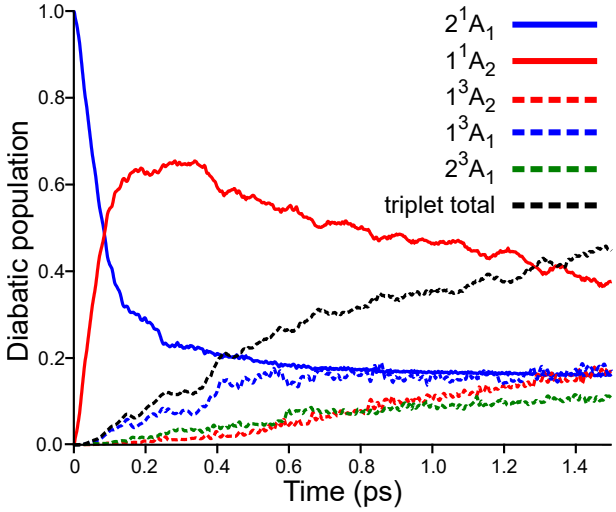

FIG. 3. Evolution of diabatic populations for the singlets 2^1A_1 ($^1\pi\pi^*$, solid blue) and 1^1A_2 ($^1n\pi^*$, solid red), and triplets 1^3A_2 ($^3n\pi^*$, dashed red), 1^3A_1 ($^3\pi\pi^*$, dashed blue) and 2^3A_1 (dashed green). The black dashed line corresponds to the sum of all triplet population. The dynamics have been started from the 2^1A_1 state.

For interpretation purposes, a kinetic mechanism can be inferred from the 1.5 ps population dynamics of Fig. 3, by fitting it to a first-order kinetic model (see Fig. S7 in the Supporting Information), taking into account that kinetic rates beyond the propagated time are extrapolated and thus less reliable. From the model, we can infer that the mechanism follows mainly a sequential transfer: $2^1A_1 \xrightarrow{IC} 1^1A_2 \xrightarrow{ISC} 1^3A_1 \xrightarrow{IC} 1^3A_2$. First, the kinetics of 2^1A_1 state decays biexponentially to the 1^1A_2 state via internal conversion. Indeed, 80% of the population of the second singlet excited state decays in a fast rate of 85 fs. This fast rate is interpreted as the first time the wavepacket reaches the $2^1A_1/1^1A_2$ crossing with a large momentum, since the path to it is barrierless. As explained, this crossing is an accidental different symmetry crossing, and thus, only activation of coupling modes of a_2 symmetry can make this transition happen, which could explain the incomplete transfer. After that, 15% of the wavepacket remains trapped in the 2^1A_1 minimum, and slowly decays to 1^1A_2 with a rate of 5 ps via the activation of coupling modes. In the 1^1A_2 state, there are two possible ISC transfers. The $1^1A_2 \rightarrow 2^3A_1$ and

$1^1A_2 \rightarrow 1^3B_2$ triplet rates are obtained at 6.73 and 44.64 respectively ps. In this time, we do not observe a fast internal conversion to the 1^3A_1 and 1^3A_2, but probably this occurs at longer times. The fastest important ISC is the $1^1A_2 \rightarrow 1^3A_1$, which is the first populated triplet in time. The rate for this transfer is given by 2.0 ps, which is probably explained by a strong spin-orbit coupling and the fact that the ISC minimum energy crossing geometry is close to the minimum of 1^1A_2 state. The internal conversion between $1^3A_1 \leftrightarrow 1^3A_2$ is the only pathway we obtained of population of the lowest triplet state, and is estimated at 602 fs for the transfer to 1^3A_2 and 803 fs for the back transfer to 1^3A_1.

In the literature, the possibility of a major channel corresponding to a "non-Kasha" transfer directly from 2^1A_1 to the 1^3A_2 triplet was evoked, first by Baba and coworkers for xanthone in the gas phase,[38,39] and later confirmed by Gilch and coworkers for xanthone in ethanol[28,29]. Baba et al. estimated the rate of transfer from 2^1A_1 in the gas phase at ca. 100 fs,[39] while the experiments of Gilch et al. in ethanol estimated it at 1.5 ps.[28] Recently, theoretical studies using rate theory in the gas phase by Rai-Constapel and coworkers predicted a 5 ps for the $2^1A_1 \rightarrow 1^3A_1$ (El-Sayed's forbidden transition), while the $2^1A_1 \rightarrow 1^3A_2$ (El-Sayed's allowed transition) was predicted to be at a rate of 200 ps.[22] In the gas phase, the main decay channel observed from 2^1A_1 is to the 1^1A_2. This is estimated at a rate of 135 fs, close to the experimental decay of 100 fs observed for 2^1A_1 in the gas phase.[39] This is due to a barrierless access to the conical intersection region between the two states. The 2^1A_1 state has an almost negligible vibronic spin-orbit coupling with energetically close 2^3A_1 and 1^3B_2 states (see Table S7 in the supporting information). The 2^3A_1 triplet receives 5-10% of the population, while the population to the 1^3B_2 states is negligible. This could explain the triplet coupling evoked for the 2^3A_1 state.[38] No direct transfer from 2^1A_1 is observed to 1^3A_2 nor 1^3A_1 states. Rather, the only important intersystem crossing channel is $1^1A_2 \rightarrow 1^3A_1$ in a rate of 2.0 ps, 10 times slower than the rate obtained by Rai-Constapel and coworkers.[22] The combined $1^1A_2 \rightarrow$triplets leads to a rate transfer of 1.5 ps. A similar rate is obtained if the dynamics are started directly from the 1^1A_2 state (see S8 in Supporting information). Finally, the transfer between $1^3A_1 \rightarrow 1^3A_2$ is fast, estimated at 602/803 fs for the forth and back transfers (in ethanol, this was estimated at 12 ps).[28] Solvents have a strong impact on the energetic order of $n\pi^*$ and $\pi\pi^*$ states of aromatic ketones, and this has a major impact on the dynamics in the excited state. Using the vacuum model, we have shifted the vertical energies to the values obtained for xanthone in solution (see Table S2 and Figure S6 in the Supporting Information). In water, the wavepacket stays trapped mainly on the singlet 1^1A_2 state, while the 2^3A_1 is the most populated among the triplets. In methanol, a slow build up of 1^1A_2 state is observed, and triplet population is negligible. Still, solvent molecules can participate in the delocalization and orientation of carbonyl's lone pair. Therefore, more general models containing solvent molecules should be constructed to simulate the excited state dynamics of xanthone in solution.

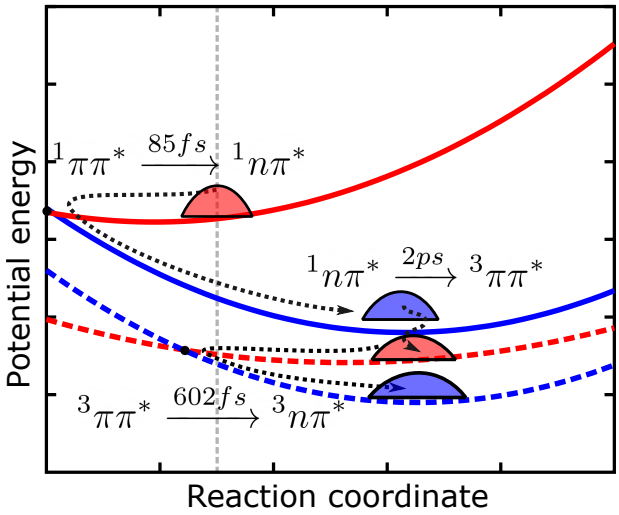

FIG. 4. Summary of the dynamical photochemical mechanism of xanthone in the gas phase starting 2^1A_1 state as extracted from quantum dynamics.

To summarize, we have developed a vibronic model for xanthone including Duschinsky effects for describing equivalently the competition between internal conversion and intersystem crossing effects in xanthone. The reaction from the quantum dynamics is summarized in Fig. 4. We determine an internal conversion of 85 fs from $^1\pi\pi \rightarrow {}^1n\pi^*$ state, followed by an intersystem crossing from $^1n\pi^* \rightarrow {}^3\pi\pi^*$ with a rate of 2.0 ps. We find no evidence of direct transfer from $^1\pi\pi^*$ to the triplets. In conclusion, this dynamical model provides one of the most complete description of xanthone to date, and can be applied in the future to clarify the internal conversion kinetics of similar aromatic ketones.

ACKNOWLEDGMENTS

MHR acknowledges financial support by the *Agence Nationale pour la Recherche* through the project BIOMAGNET (ANR-16CE29-0008-01). Centre de Calcul Intensif d'Aix-Marseille is acknowledged for granting access to its high performance computing resources. MAR and CdG acknowledge the Spanish ministry of Science and Innovation (Project PID2020-113187GB-I00) and the Generalitat de Catalunya (project 2017-SGR629) for financial support.

DATA AVAILABILITY

The data that support the findings of this study are available from the corresponding author upon reasonable

request.

[1] D. R. Kearns and W. A. Case, J. Am. Chem. Soc. **88**, 5087 (1966).
[2] R. N. Griffin, Photochemistry and Photobiology **7**, 159 (1968).
[3] D. E. Damschen, C. D. Merritt, D. L. Perry, G. W. Scott, and L. D. Talley, J. Phys. Chem. **82**, 2268 (1978).
[4] G. Scharf and J. Winefordner, Talanta **33**, 17 (1986).
[5] M. A. El-Sayed, J. Chem. Phys. **38**, 2834 (1963).
[6] S. T. Park, J. S. Feenstra, and A. H. Zewail, J. Chem. Phys. **124**, 174707 (2006).
[7] S. Aloïse, C. Ruckebusch, L. Blanchet, J. Réhault, G. Buntinx, and J.-P. Huvenne, J. Phys. Chem. A **112**, 224 (2008).
[8] T. Kobayashi and S. Nagakura, Chem. Phys. Lett. **43**, 429 (1976).
[9] G. Spighi, M.-A. Gaveau, J.-M. Mestdagh, L. Poisson, and B. Soep, Phys. Chem. Chem. Phys. **16**, 9610 (2014).
[10] B. Soep, J.-M. Mestdagh, M. Briant, M.-A. Gaveau, and L. Poisson, Phys. Chem. Chem. Phys. **18**, 22914 (2016).
[11] C.-W. Chang, T. I. Sølling, and E. W.-G. Diau, Chem. Phys. Lett. **686**, 218 (2017).
[12] J. C. Scaiano, J. Am. Chem. Soc. **102**, 7747 (1980).
[13] J. J. Cavaleri, K. Prater, and R. M. Bowman, Chem. Phys. Lett. **259**, 495 (1996).
[14] C. Ley, F. Morlet-Savary, J. Fouassier, and P. Jacques, J. Photochem. Photobiol. A **137**, 87 (2000).
[15] C. Ley, F. Morlet-Savary, P. Jacques, and J. Fouassier, Chemical Physics **255**, 335 (2000).
[16] I. Ghosh, A. Mukhopadhyay, A. L. Koner, S. Samanta, W. M. Nau, and J. N. Moorthy, Phys. Chem. Chem. Phys. **16**, 16436 (2014).
[17] C. W. Ashpole, S. J. Formosinho, and G. Porter, Proceedings of the Royal Society of London. Series A, Mathematical and Physical Sciences **323**, 11 (1971).
[18] N. S. Hill and M. L. Coote, J. Am. Chem. Soc. **140**, 17800 (2018).
[19] S. Rani, J. Sobhanadri, and T. Prasada Rao, J. Photochem. Photobiol. A **94**, 1 (1996).
[20] W. Domcke, D. Yarkony, and H. Koppel, eds., Conical Intersections: Theory, Computation and experiment, Advanced Series in Physical Chemistry, Vol. 17 (World Scientific Publishing Co Pte Ltd, 2011).
[21] N. Ohmori, T. Suzuki, and M. Ito, J. Phys. Chem. **92**, 1086 (1988).
[22] V. Rai-Constapel, M. Etinski, and C. M. Marian, J. Phys. Chem. A **117**, 3935 (2013).
[23] M. Huix-Rotllant, I. Burghardt, and N. Ferré, Comptes Rendus Chimie **19**, 50 (2016).
[24] L. Favero, G. Granucci, and M. Persico, Phys. Chem. Chem. Phys. **18**, 10499 (2016).
[25] V. Rai-Constapel, M. Kleinschmidt, S. Salzmann, L. Serrano-Andrés, and C. M. Marian, Phys. Chem. Chem. Phys. **12**, 9320 (2010).
[26] V. Rai-Constapel, S. Salzmann, and C. M. Marian, J. Phys. Chem. A **115**, 8589 (2011).
[27] R. Mundt, T. Villnow, C. T. Ziegenbein, P. Gilch, C. Marian, and V. Rai-Constapel, Phys. Chem. Chem. Phys. **18**, 6637 (2016).
[28] H. Satzger, B. Schmidt, C. Root, W. Zinth, B. Fierz, F. Krieger, T. Kiefhaber, and P. Gilch, J. Phys. Chem. A **108**, 10072 (2004).
[29] B. Heinz, B. Schmidt, C. Root, H. Satzger, F. Milota, B. Fierz, T. Kiefhaber, W. Zinth, and P. Gilch, Phys. Chem. Chem. Phys. **8**, 3432 (2006).
[30] B. Heinz, B. Schmidt, C. Root, F. Milota, B. Fierz, T. Kiefhaber, W. Zinth, and P. Gilch, in Ultrafast Phenomena XV, edited by P. Corkum, D. M. Jonas, R. J. D. Miller, and A. M. Weiner (Springer Berlin Heidelberg, Berlin, Heidelberg, 2007) pp. 513–515.
[31] M. Bracker, C. M. Marian, and M. Kleinschmidt, J. Chem. Phys. **155**, 014102 (2021).
[32] T. E. Sharp and H. M. Rosenstock, J. Chem. Phys. **41**, 3453 (1964).
[33] A. Thöny and M. J. Rossi, J. Photochem. Photobiol. A **104**, 25 (1997).
[34] E. J. Heller, J. Chem. Phys. **68**, 2066 (1978).
[35] V. Engel, Chem. Phys. Lett. **189**, 76 (1992).
[36] F. Santoro, R. Improta, A. Lami, J. Bloino, and V. Barone, J. Chem. Phys. **126**, 084509 (2007).
[37] F. Santoro, A. Lami, R. Improta, J. Bloino, and V. Barone, J. Chem. Phys. **128**, 224311 (2008).
[38] M. Baba, T. Kamei, M. Kiritani, S. Yamauchi, and N. Hirota, Chem. Phys. Lett. **185**, 354 (1991).
[39] Y. Ohshima, T. Fujii, T. Fujita, D. Inaba, and M. Baba, J. Phys. Chem. A **107**, 8851 (2003).